Applied Physics A (2020) 126:446
https://doi.org/10.1007/s00339-020-03640-0

Applied Physics A
Materials Science & Processing

S.I. : CURRENT STATE-OF-THE-ART IN LASER ABLATION

Pulse duration dependence of ablation threshold for fused silica in the visible femtosecond regime

E. Terasawa[1,2] · T. Shibuya[3] · D. Satoh[2,3] · Y. Moriai[2] · H. Ogawa[2,3] · M. Tanaka[2,3] · R. Kuroda[2,3] · Y. Kobayashi[2,4] · K. Sakaue[1,5] · M. Washio[1]

Received: 15 October 2019 / Accepted: 15 May 2020 / Published online: 25 May 2020

Abstract
In this study, we investigated the variation of the femtosecond pulse duration of the threshold fluence of fused silica by a single-shot irradiation at a wavelength of 400 nm. The single-shot threshold fluence was obtained from the relationship between the crater area based on the crater shape and the irradiation fluence. The crater shape was divided into two affected regimes depending on the pulse duration and the laser fluence. The crater depth and each threshold fluence for the corresponding two affected regimes were also measured. We have found that shorter pulse duration provides more energy-efficient results.

Keywords Laser ablation · Femtosecond laser · Ablation threshold · Pulse duration dependence · Fused silica · Visible wavelength

1 Introduction

The ablation phenomenon induced by ultrashort laser pulses has attractive properties and is an important research area both scientifically and industrially [1, 2]. Compared to conventional laser processing by the heat melting process, the main advantage of the ablation phenomenon is high-precision and high-quality processing caused by a significant reduction in the heat-affected zone [1, 2].

Fused silica is a dielectric material, for which high-quality processing is expected by the ultrashort laser pulse. Several studies on the ablation phenomenon mechanism of dielectrics containing fused silica by ultrashort laser pulses were conducted [3–6]. The ultrashort laser ablation of the dielectric can be classified into two types [7–15]: (1) a 'gentle' ablation phase, where the ablation efficiency is low, and (2) a 'strong' ablation phase, where the ablation efficiency is high, and the melting traces (e.g. droplets) are confirmed. The gentle ablation is caused by the Coulomb explosion [8, 9, 11, 12] or material densification [13], whilst the strong ablation is caused by phase explosion [16, 17].

The threshold fluence is used in a manner similar to the critical points for a laser-induced breakdown of optical components, application to micromachining, and quantitative comparisons with a theoretical model. However, the threshold fluence in the ultrashort pulse region is mainly measured in the near-infrared wavelength region [3, 6, 18–21], and only a few studies performed measurements in the shorter wavelength region [18, 22]. The present study determined the single-shot threshold fluence of fused silica in the 100–700 fs range at 400 nm wavelength. The ablated crater by the single-shot irradiation was divided into two affected regimes. The thresholds of the two affected regimes were measured from the relationship between the laser fluence and the affected area of the crater. Each single-shot threshold fluence and the pulse duration dependence were obtained.

✉ E. Terasawa
wisdom_terasawa@akane.waseda.jp

[1] Waseda Research Institute for Science and Engineering, Waseda University, 3-4-1 Okubo, Shinjuku, Tokyo, Japan

[2] OPERANDO-OIL, National Institute of Advanced Industrial Science and Technology (AIST), 5-1-5 Kashiwanoha, Kashiwa, Chiba, Japan

[3] RIMA, National Institute of Advanced Industrial Science and Technology (AIST), Central 2, 1-1-1 Umezono, Tsukuba, Ibaraki, Japan

[4] The Institute for Solid State Physics, The University of Tokyo, 5-1-5 Kashiwanoha, Kashiwa, Chiba, Japan

[5] Photon Science Center, Graduate School of Engineering, The University of Tokyo, 7-3-1 Hongo, Bunkyo, Tokyo, Japan

2 Experimental

2.1 Experimental arrangements

The laser source used in this experiment was a Ti:sapphire laser amplifier based on chirped pulse amplification, which delivered 1 kHz and 3.0 mJ pulses at 800 nm. The fundamental wave of 800 nm was converted into a harmonic wave of 400 nm in a lithium triborate crystal. The pulse duration could be controlled by varying the diffraction grating distance in the 100–700 fs range. The pulse duration was measured using an autocorrelation method. The laser was linearly polarised, and the energy was varied using a half-wave plate. A thin-film polariser was used at the Brewster angle. The energy per pulse of the laser beam was measured based on the reflected light from the thin-film polariser. The energy distribution was a Gaussian beam. After focusing on the sample's surface using a plano-convex lens with 100 mm focal length, the beam waist radii ($1/e^2$) were obtained as approximately $\omega_x = 4.2$ µm and $\omega_y = 3.9$ µm through the Liu plot [23] for each pulse duration.

Synthetic fused silica (10 mm × 10 mm × 0.5 mm, double-sided mirror surface), which is a widely studied transparent dielectric material, was used as the sample. The sample was positioned on a 3-axis motorised stage controlled with ≤ 50 nm accuracy. All irradiations were performed using a single shot in the air to eliminate the influence of the incubation effect. The crater areas used in the Liu plot were measured using a laser confocal microscope (KEYENCE, VK-X250). The crater shapes with more details were observed using atomic force microscopy (AFM, Park Systems, NX10).

2.2 Threshold fluence measurement method

The threshold fluence was measured using the Liu plot [23–25]. The measurement method was based on the dependence of the crater area on the laser pulse fluence. The fluence spatial distribution of the Gaussian beam at the focal position can be expressed as

$$F(r) = F_{\text{peak}} \exp\left(-\frac{2r^2}{\omega_0^2}\right), \tag{1}$$

where the peak laser fluence is $F_{\text{peak}} = 2E_{\text{pulse}}/\omega_0^2$; E_{pulse} is the pulse energy; r is the position from the centre of the beam; and ω_0 is the beam waist radius. The fluence $F(r)$ is the threshold fluence if in the distribution, where damage is observed, no damage is found at a given r from the centre ($r = 0$) for the first time. The interaction between the laser pulse and the sample is described as follows: the crater diameter, D, is logarithmically proportional with the laser pulse fluence function $F(r)$ given as

$$D^2 = 2\omega_0^2 \ln\left(\frac{F_{\text{peak}}}{F_{\text{th}}}\right), \tag{2}$$

where F_{th} is the peak fluence threshold. The fluence at which the linear approximation is $D^2 = 0$ is defined as the threshold fluence F_{th} by numerical regression. The shape of the processing mark in this work (Fig. 1) was slightly elliptical (ellipticity ~ 0.9); thus, the beam shape was slightly elliptical. The beam shape was assumed to be a circle. The threshold was determined from the Liu plot by substituting D_xD_y in D^2 in Eq. (2). The Liu plot results showed approximately $\omega_0 = 4.0$ µm for each pulse duration.

3 Results and discussion

Figure 1a–c shows the shapes of the single-shot crater measured by AFM. Figure 1d–f depicts the cross section at the major axis. The crater irradiated by a 100-fs pulse at 6.71 J/cm^2 (Fig. 1a, d) was approximately 4.4 µm wide and 200 nm deep and has distinct rim structures at the edge. In contrast, the crater irradiated by a 600-fs pulse at 6.00 J/cm^2 (Fig. 1b, e) was approximately 3.3 µm wide and 40 nm deep. It had no rim and had a shallow depression shape. Even with nearly the same energy, the crater shape noticeably varied depending on the pulse duration. Figure 1c, f shows a crater formed when only the fluence was increased from 6.00 J/cm^2 (Fig. 1b, e) to 11.8 J/cm^2 with the 600-fs pulse. As shown in Fig. 1f, this crater has a rim at $x = \pm 2$ µm, and outside of the rim is the affected area.

The single-shot threshold fluences were determined using the Liu plot in the pulse duration region of 100–700 fs at every 100 fs. The major and minor axes of the crater used in the Liu plot were distinguished by two affected areas. If the edge of the crater has a rim structure, the major D_{x_1} and the minor D_{y_1} axes of the affected zone are defined as the distance between the highest points of the rim. If no rim structure exists at the edge of the crater, the major D_{x_2} and minor D_{y_2} axes of the affected zone are defined as the distance between the points where the sample surface clearly starts to be depressed. Figure 1d–f shows the definitions of D_{x_1}, D_{y_1}, D_{x_2}, and D_{y_2}. The crater shape applied in the Liu plot was measured using a laser confocal microscope. The two craters in Fig. 1c–f were measured using a laser confocal microscope like those of the AFM measurement, which confirmed that the results were nearly the same as those of AFM.

Figure 2 presents examples of the results by plotting the crater area D_xD_y as a function of the laser fluence for each

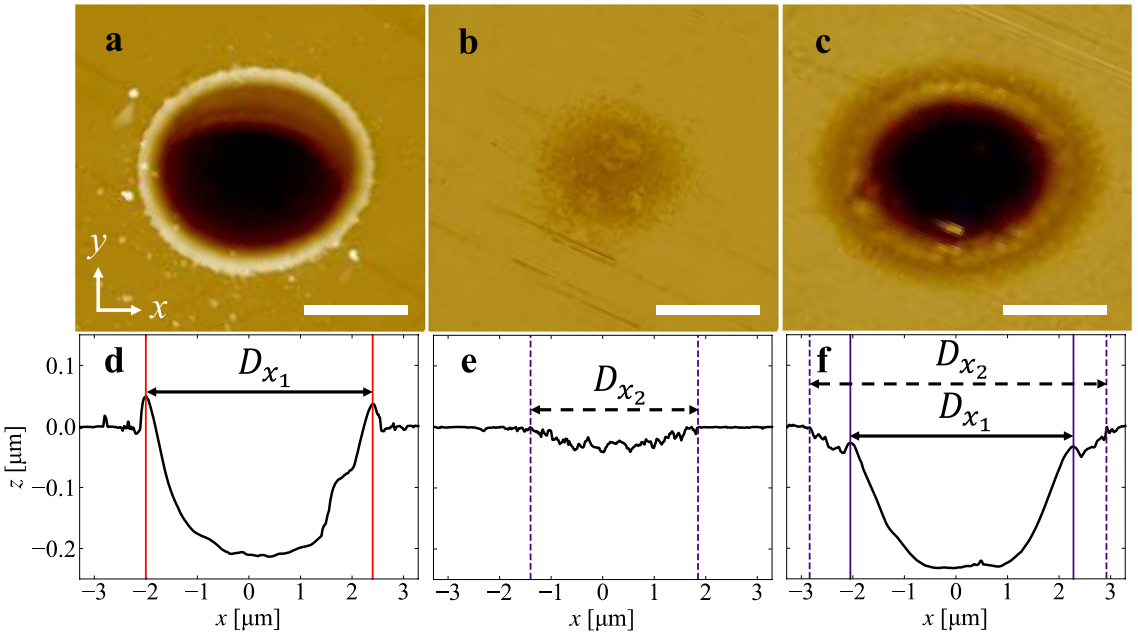

Fig. 1 AFM images of the craters generated on the fused silica for single pulse of different pulse durations τ and fluence F_{peak} values: **a** $\tau = 100$ fs, $F_{peak} = 6.71$ J/cm^2, **b** $\tau = 600$ fs, $F_{peak} = 6.00$ J/cm^2, and **c** $\tau = 600$ fs, $F_{peak} = 11.8$ J/cm^2. Cross sections **d**–**f** in the major axis direction correspond to the images in panels **a**–**c**, respectively. The white bar represents 2 μm

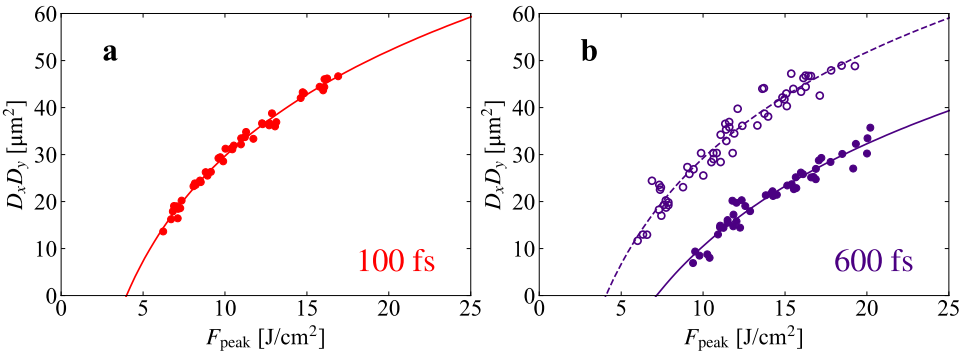

Fig. 2 Crater area D_xD_y as a function of the laser fluence F_{peak} at each pulse duration: τ: **a** $\tau = 100$ fs and **b** $\tau = 600$ fs. The filled and empty circles represent the affected areas of $D_{x_1}D_{y_1}$ and $D_{x_2}D_{y_2}$, respectively

pulse duration with a fluence range of approximately 5–25 J/cm^2. In pulse durations of 100 fs (Fig. 2a), 200 fs, and 300 fs, the affected area with the rim structure was confirmed, but different affected zones outside the rim structure could not be clearly identified. In the pulse durations of 400 fs, 500 fs, 600 fs (Fig. 2b), and 700 fs, two affected areas were confirmed by the fluence. Each plot was fitted using Eq. (2). The solid line fittings show the crater shape of $D_{x_1}D_{y_1}$. The dotted line fittings depict the crater shape of $D_{x_2}D_{y_2}$.

Figure 3 shows the dependence of the single-shot ablation threshold on the pulse duration. The ablation threshold was distinguished from F_{th_1} and F_{th_2} by the affected areas. F_{th_1} was measured at every pulse duration. F_{th_1} is a value in the range of 4–7 J/cm^2, which strongly depended on the pulse duration and decreased from 7 to 4 J/cm^2 as the pulse duration decreased. F_{th_2} was measured only at the pulse durations

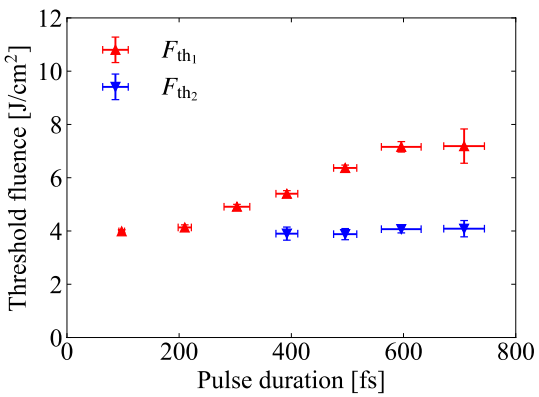

Fig. 3 Dependence of the single-shot threshold fluence on the pulse duration at the 400 nm wavelength. The red and blue triangles indicate F_{th_1} and F_{th_2}, respectively

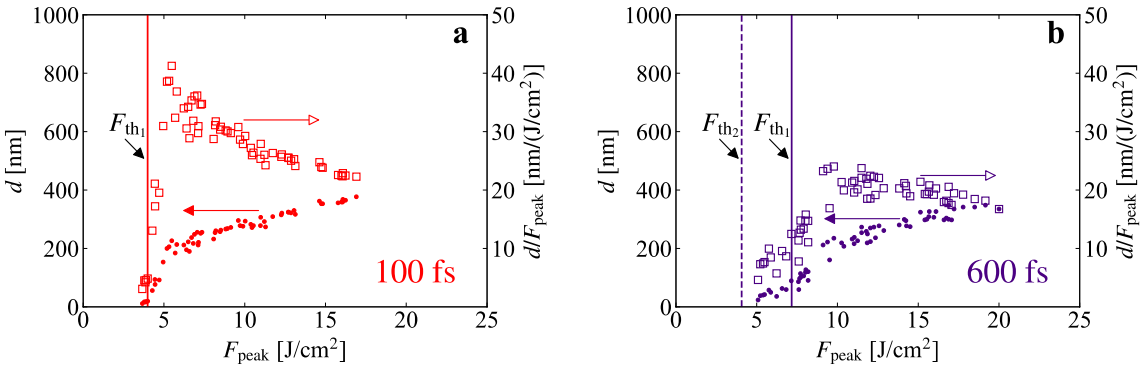

Fig. 4 Crater depth d and ablation efficiency d/F_{peak} as a function of the laser fluence F_{peak} at each pulse duration: τ: **a** $\tau = 100$ fs and **b** $\tau = 600$ fs. The filled circles represent the crater depth d on the left axis. The empty squares represent the ablation efficiency d/F_{peak} on the right axis. The solid and dotted vertical lines show the threshold fluences F_{th_1} and F_{th_2} from Fig. 2, respectively

in the 400–700 fs range. F_{th_2} had a nearly constant value of ~4 J/cm^2 for any pulse duration.

The obtained thresholds are discussed with only the data of the affected area of the crater. Therefore, we measured the crater depth. The crater depth measurements were made with a laser confocal microscope, which confirmed that the results were nearly the same as those of AFM. Figure 4 shows the results of the ablation depth d and ablation efficiency d/F_{peak}. In the figure, the measured threshold fluence is shown by a vertical straight line. The maximum ablation efficiencies of 100 fs and 600 fs were achieved at approximately 6 J/cm^2 and 10 J/cm^2, respectively. Both results showed the maximum ablation efficiencies at the fluences in this range just above the threshold fluence of F_{th_1}. Moreover, the maximum ablation efficiency was higher at 100 fs than at 600 fs, and the fluence achieved was lower. This result indicates that the shorter pulse duration is more efficient for the ablation depth in this energy range.

The significance of the two threshold fluences obtained herein must be discussed. The ablation efficiency increased at fluences above F_{th_1}. The ablation depth saturated above the maximum ablation efficiency. This result is similar to the multi-shot ablation phenomenon, where the ablation efficiency increases when a certain number of shots are exceeded [7, 8], and suggests that F_{th_1} is the strong ablation threshold fluence caused by the phase explosion. The presence of the rim used to define the threshold fluence F_{th_1} is one reason for the phase change indicating the presence of a molten layer [26, 27]. Conversely, F_{th_2}, which was located in the area with a lower fluence than F_{th_1}, was considered the gentle ablation threshold fluence. Several studies reported that the surface becomes rougher as the number of shots increases, and strong ablation occurs [8]; however, this study found that the surface of the crater bottom in the fluence region above F_{th_1} was relatively smooth. The surface roughness trend is different from the multi-shot ablation, and further investigation is required.

4 Conclusions

We determined the single-shot threshold fluence of fused silica in the femtosecond pulse duration range at 400 nm wavelength. Two affected areas of the crater were measured using single-shot irradiation depending on the pulse duration and fluence. The dependence of the two ablation thresholds (F_{th_1}, F_{th_2}) on the pulse duration was also determined. The pulse duration dependences of the two ablation thresholds (F_{th_1}, F_{th_2}) showed a different trend. In addition, the crater depth by the single-shot irradiation was measured. The depth of the ablated craters showed that the shorter pulse duration was more efficient.

Acknowledgements This work is partly based on the results obtained from the New Energy and Industrial Technology Development Organization (NEDO) Project (Grant No. P16011) 'Development of advanced laser processing with intelligence based on high-brightness and high-efficiency laser technologies' (TACMI Project).

References

1. A.Y. Vorobyev, C. Guo, Laser Photonics Rev. **7**, 385 (2013)
2. K. Sugioka, Y. Cheng, Light Sci. Appl. **3**, e149 (2014)
3. M. Lenzner, J. Krüger, S. Sartania, Z. Cheng, C. Spielmann, G. Mourou, F. Kautek, Phys. Rev. Lett. **80**, 4076 (1998)
4. B. Stuart, M. Feit, S. Herman, A. Rubenchik, B. Shore, M. Perry, Phys. Rev. B **53**, 1749 (1996)
5. M. Lebugle, N. Sanner, O. Utéza, M. Sentis, Appl. Phys. A Mater. Sci. Process. **114**, 129 (2014)
6. B. Chimier, O. Utéza, N. Sanner, M. Sentis, T. Itina, P. Lassonde, F. Légaré, F. Vidal, J.C. Kieffer, Phys. Rev. B **84**, 094104 (2011)
7. A.C. Tam, J.L. Brand, D.C. Cheng, W. Zapka, Appl. Phys. Lett. **55**, 2045 (1989)
8. D. Ashkenasi, A. Rosenfeld, H. Varel, M. Wähmer, E.E.B. Campbell, Appl. Surf. Sci. **120**, 65 (1997)
9. D. Ashkenasi, R. Stoian, A. Rosenfeld, Appl. Surf. Sci. **154**, 40 (2000)

10. S. Guizard, A. Semerok, J. Gaudin, M. Hashida, P. Martin, F. Quéré, Appl. Surf. Sci. **186**, 364 (2002)
11. R. Stoian, D. Ashkenasi, A. Rosenfeld, E.E.B. Campbell, Phys. Rev. B **62**, 13167 (2000)
12. R. Stoian, A. Rosenfeld, D. Ashkenasi, I.V. Hertel, N.M. Bulgakova, E.E. Campbell, Phys. Rev. Lett. **88**, 097603 (2002)
13. J. Siegel, D. Puerto, W. Gawelda, G. Bachelier, J. Solis, L. Ehrentraut, J. Bonse, Appl. Phys. Lett. **91**, 082902 (2007)
14. D. Puerto, J. Siegel, W. Gawelda, M. Galvan-Sosa, L. Ehrentraut, J. Bonse, J. Solis, J. Opt. Soc. Am. B **27**, 1065 (2010)
15. L. Qi, K. Nishii, M. Yasui, H. Aoki, Y. Namba, Opt. Lasers Eng. **48**, 1000 (2010)
16. S. Eliezer, N. Eliaz, E. Grossman, D. Fisher, I. Gouzman, Z. Henis, S. Pecker, Y. Horovitz, M. Fraenkel, S. Maman, Y. Lereah, Phys. Rev. B **69**, 144119 (2004)
17. J. Perrière, C. Boulmer-Leborgne, R. Benzerga, S. Tricot, J. Phys. D Appl. Phys. **40**, 7069 (2007)
18. M.D. Perry, B.C. Stuart, P.S. Banks, M.D. Feit, V. Yanovsky, A.M. Rubenchik, J. Appl. Phys. **85**, 6803 (1999)
19. D. Du, X. Liu, G. Korn, J. Squier, G. Mourou, Appl. Phys. Lett. **64**, 3071 (1994)
20. H. Varel, D. Ashkenasi, A. Rosenfeld, R. Herrmann, F. Noack, E.E.B. Campbell, Appl. Phys. A **62**, 293 (1996)
21. A.C. Tien, S. Backus, H. Kapteyn, M. Murnane, G. Mourou, Phys. Rev. Lett. **82**, 3883 (1999)
22. T.Q. Jia, Z.Z. Xu, X.X. Li, R.X. Li, B. Shuai, F.L. Zhao, Appl. Phys. Lett. **82**, 4382 (2003)
23. J.M. Liu, Opt. Lett. **7**, 196 (1982)
24. N. Sanner, O. Utéza, B. Bussiere, G. Coustillier, A. Leray, T. Itina, M. Sentis, Appl. Phys. A **94**, 889 (2009)
25. A. Ben-Yakar, R.L. Byer, J. Appl. Phys. **96**, 5316 (2004)
26. A. Ben-Yakar, R.L. Byer, A. Harkin, J. Ashmore, H.A. Stone, M. Shen, E. Mazur, Appl. Phys. Lett. **83**, 3030 (2003)
27. A. Ben-Yakar, A. Harkin, J. Ashmore, R.L. Byer, H.A. Stone, J. Phys. D Appl. Phys. **40**, 1447 (2007)